Colloids and Surfaces A: Physicochem. Eng. Aspects 480 (2015) 296–306

Contents lists available at ScienceDirect

Colloids and Surfaces A: Physicochemical and Engineering Aspects

journal homepage: www.elsevier.com/locate/colsurfa

Behavior of pyrene as a polarity probe in palmitoylsphingomyelin and palmitoylsphingomyelin/cholesterol bilayers: A molecular dynamics simulation study

António M.T.M. do Canto[a], Patrícia D. Santos[a], Jorge Martins[b], Luís M.S. Loura[c,d,*]

[a] Centro de Química de Évora, Departamento de Química, Escola de Ciências e Tecnologia, Universidade de Évora, Rua Romão Ramalho, 59, 7000-671 Évora, Portugal
[b] IBB-CBME and DCBB-FCT, Universidade do Algarve, Campus de Gambelas, 8005-139 Faro, Portugal
[c] Faculdade de Farmácia, Universidade de Coimbra, Pólo das Ciências da Saúde, Azinhaga de Santa Comba, 3000-548 Coimbra, Portugal
[d] Centro de Química de Coimbra, Universidade de Coimbra, Rua Larga, 3004-535 Coimbra, Portugal

HIGHLIGHTS

- *N*-Palmitoylsphingomyelin/cholesterol bilayers are simulated in presence of pyrene.
- The presence of pyrene does not affect the host bilayer properties significantly.
- Pyrene dynamics are considerably slowed down by the addition of cholesterol.
- Pyrene location inside the bilayer hydrocarbon region is not affected by cholesterol.
- However, pyrene hydration is reduced upon increasing the cholesterol concentration.

GRAPHICAL ABSTRACT

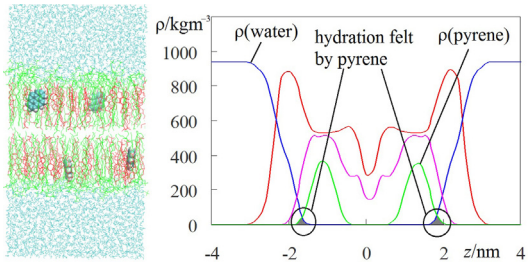

ARTICLE INFO

Article history:
Received 25 June 2014
Received in revised form 5 December 2014
Accepted 7 December 2014
Available online 16 December 2014

Keywords:
Cholesterol
Lipid bilayer
Molecular dynamics
Polarity
Pyrene
Sphingomyelin

ABSTRACT

Pyrene is a polycyclic aromatic hydrocarbon noted for its remarkable optical spectroscopic properties. Among its uses as a fluorescent probe, measurement of lipid bilayer's equivalent polarity through the pyrene Ham effect stands out. To this effect, the ratio of the intensities of the first and third vibronic bands (I_1/I_3) in its emission spectrum of pyrene is measured. However, issues concerning the precise location of bilayer-inserted pyrene and the possibility of probe-induced perturbation of host bilayer properties are potential sources of concern in this regard. Atomistic molecular dynamics simulations constitute a useful method for the characterization of lipid membrane systems, and, in particular, to understand the behavior of fluorescence probes upon incorporation in lipid bilayers. In this report, we present a detailed characterization of the behavior of pyrene in fluid *N*-palmitoylsphingomyelin (PSM) and PSM/cholesterol membranes, with emphasis on the degree of proximity between the probe and water molecules inside bilayers, related to the use of pyrene to measure equivalent lipid bilayer polarity. It is concluded that pyrene exerts minor effects on bilayer properties, with slight local disordering being apparent for high

Abbreviations: ACF, autocorrelation function; Chol, cholesterol; DPPC, dipalmitoylphosphatidylcholine; MD, molecular dynamics; MSD, mean squared displacement; PC, phosphatidylcholine; POPC, 1-palmitoyl-2-oleoyl-*sn*-glycero-3-phosphocholine; PSM, *N*-palmitoylsphingomyelin; SM, sphingomyelin.

* Corresponding author at: Faculdade de Farmácia, Universidade de Coimbra, Pólo das Ciências da Saúde, Azinhaga de Santa Comba, 3000-548 Coimbra, Portugal. Tel.: +351 239 488 485; fax: +351 239 488 503.
E-mail address: lloura@ff.uc.pt (L.M.S. Loura).

http://dx.doi.org/10.1016/j.colsurfa.2014.12.012

cholesterol content. Whereas rotation and lateral diffusion of pyrene are greatly slowed in cholesterol-rich systems, its relative transverse location is not significantly affected. While hydration of PSM bilayers, as sensed by pyrene, is already low compared to that of fluid phosphatidylcholine, it becomes even smaller for high cholesterol mole fraction at the studied temperature.

1. Introduction

Phospholipid bilayers are the basic structural units of biological membranes, demarcating the interior and exterior of cells and their organelles. As models of biological membranes, lipid bilayers have been a major research topic in biophysical chemistry [1,2]. One of their most important properties is their hydration or polarity profile, which shapes the hydrophobic membrane barrier [3], and thereby constitutes an energetic determinant for insertion of peptides, proteins and amphiphilic molecules, as well as for transport of both polar and apolar solutes across the bilayer [4].

Several techniques based on fluorescence spectroscopy are available for the estimation of polarity in lipid bilayers, exploiting the environmental sensitivity of extrinsic probes, such as prodan, laurdan, dansyl, or anthroyl labeled probes (e.g. [5,6]). Among these methodologies, one that has been surprisingly seldom used in membrane systems is that based on the Ham effect of pyrene [7], the so-called *Py* scale of equivalent polarity [8,9]. Pyrene is a polycyclic aromatic hydrocarbon noted for its remarkable fluorescence properties, such as an unusually long excited-state lifetime (>100 ns in a variety of aerated solvents and micellar or model membrane systems), emission spectrum highly sensitive to solvent polarity and concentration-dependent and/or viscosity-influenced excimer formation [10]. The *Py* scale of polarity is based on the measurement of the ratio of the fluorescence intensities of the first and third vibronic bands (I_1/I_3) in the spectra of pyrene. Previously, we demonstrated the application of this scale to lipid bilayers composed of phosphatidylcholine (PC), both in presence and absence of cholesterol (Chol) [11].

However, there are two crucial issues regarding use of extrinsic membrane probes, and pyrene in particular: what is their precise location within the bilayer (and thus what region they report on), and whether they induce significant perturbation on the host bilayer properties. For this purpose, molecular dynamics (MD) simulations have been useful to characterize simultaneously membrane probe behavior and probe-induced perturbation with atomic detail, for several classes of fluorescent lipophilic probes (see [12,13] for reviews), including free pyrene [14,15]. Recently, we carried out MD simulations of pyrene in 1-palmitoyl-2-oleoyl-*sn*-glycero-3-phosphocholine (POPC) bilayers, with varying amounts of Chol [16]. This work was valuable in the clarification of the use of the pyrene Ham Effect to effectively measure equivalent polarity in mixed lipid bilayers containing unsaturated PC and Chol.

In this report, we extend our previous MD study by applying this methodology to the study of pyrene inside *N*-palmitoyl-sphingomyelin (PSM)/Chol bilayers (structures are shown in Fig. 1, together with that of pyrene). Alongside PC and Chol, sphingosine-based sphingomyelin (SM) is a major component of mammalian plasma membranes, and is particularly relevant as (together with Chol) the main constituent of lipid rafts, specialized membrane domains implicated in processes including cellular signaling and trafficking [17–19]. SM chains typically display a larger degree of saturation and higher main transition temperature compared to other lipid classes [2]. For this reason, and because of their ability to form a network of intermolecular hydrogen bonds involving their amide and/or hydroxyl groups, SM-enriched membrane domains are highly ordered. This also applies to rafts, in which the ordering effects of Chol contribute to create a very tight molecular packing. To investigate if pyrene is well accommodated within SM/Chol bilayers, its precise location and effect on membrane properties, and to gain insights on the polarity sensed by the probe in these systems, we carried out extensive (300–400 ns) simulations of PSM/Chol bilayers (0 mol%, 5 mol%, 20 mol%, 40 mol%, 45 mol% and 50 mol% of the latter component). The determination of bilayer polarity corresponding to rafts enriched in SM/Chol is relevant for the understanding of the solvation properties of lipid bilayers, that may influence the structure and functioning of proteins associated to domain-limited biochemical reactions and processes. In bilayer hydration terms, it is expected that bilayer domains enriched in PSM, but with low Chol content ($\leq$5 mol%) are of significantly higher polarity than those domains containing upper Chol proportions (20 mol% $\leq$ Chol content $\leq$ 50 mol%). When changing the proportion of Chol in PSM bilayers, subtle changes in bilayer hydration are revealed, together with the effects of pyrene in the bilayer ordering and dynamics of the lipidic components, studied at the atomic resolution. Besides the intrinsic less fluid characteristics of bilayer domains enriched in PSM/Chol mixtures, there are unequivocal variations in bilayer hydration that must be taken into account when analyzing membrane phenomena involving the specialized raft domains.

2. Methods

MD simulations and analysis of trajectories were carried out using the GROMACS 4.6.3 package [20–22]. PSM united-atom structure and topology, as used by Niemelä et al. [23], were obtained through the Lipidbook web page [24]. Chol united atom structure and topology were adapted from those of Höltje et al. [25] (available for download at the GROMACS webpage [26]) by changing the molecule types from CH2/CH3 to LP2/LP3, to avoid overcondensation of the bilayer, as described and tested elsewhere [27]. Pyrene was parameterized as described by Hoff [14,28]. Bilayer models with varying numbers (shown in Table 1) of PSM and Chol molecules were assembled using GROMACS 4.6.3 tools, and fully hydrated with SPC water [29]. For the simulations with incorporated probe, initial structures with 2 or 4 pyrene molecules (one or two in each leaflet, respectively) were then obtained by randomly inserting probe molecules inside a PSM or PSM/Chol bilayer without replacement of lipids.

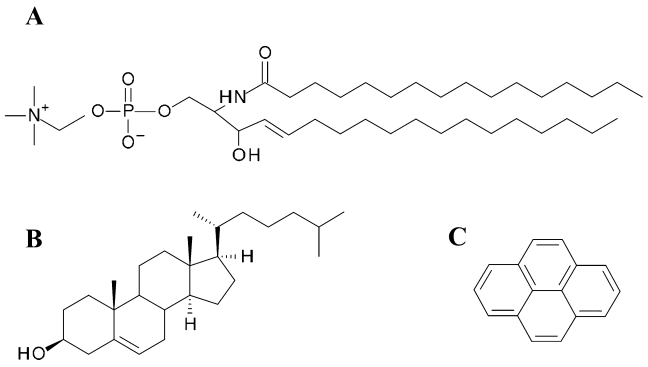

Fig. 1. Structures of PSM (A), Chol (B), and pyrene (C).

Table 1
Composition of the systems studied in the present work.

Chol mole fraction	n_{PSM}	n_{Chol}	$n_{water}/(n_{PSM}+n_{Chol})$
0	144	–	32.9
5	152	8	37.7
20	120	30	32.2
40	90	60	31.4
45	72	60	34.8
50	72	72	32.9

Prior to the full MD simulation, all systems underwent a steepest-descent energy minimization of the structure, followed by a small MD run (100 ps) to properly allow the solvent molecules to adjust and/or relax around the membrane. Extensive molecular dynamics simulations (300 ns for 0, 5, and 20 mol% Chol, 400 ns for 40, 45, and 50 mol% Chol) were then carried out under constant number of particles, pressure and temperature, and using periodic boundary conditions. Pressure (semi-isotropic, 1 bar, 1.0 ps coupling time) and temperature (333 K, 0.1 ps coupling time) control was carried out using the weak-coupling Berendsen schemes [30]. The temperature, well above the reported value for the main transition of PSM (~314 K [2]), was chosen to ensure that bilayers were in a proper liquid-crystalline state. All bond lengths were constrained to their equilibrium values using the SETTLE algorithm [31] for water and the LINCS algorithm [32] for all other bonds. An integration time step of 2 fs was used. Van der Waals interactions were cut off at 1.0 nm. Coulomb interactions were calculated using the Particle Mesh Ewald method [33], with a cut-off of 1.0 nm for the real space component. For visualization of structures/trajectories, Visual Molecular Dynamics software (University of Illinois) was used [34].

3. Results and discussion

3.1. Molecular areas

Fig. 2 depicts the evolution of the molecular areas of PSM and Chol for all studied systems (calculated using the method of Hofsäß et al. [35]), while Fig. 3 illustrates the final configurations in each

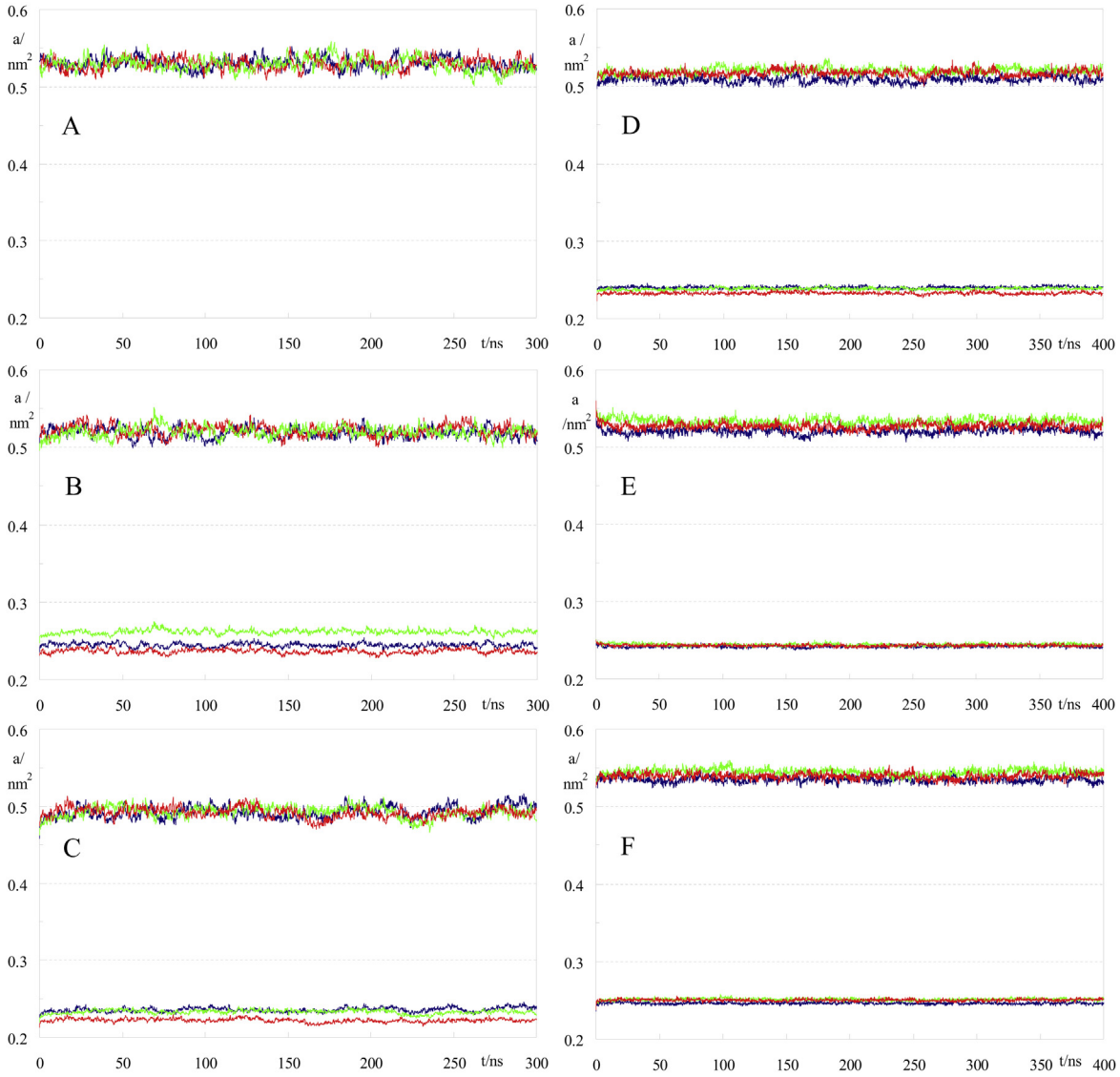

Fig. 2. Time variations of the molecular areas of PSM (in the 0.45–0.6 nm^2 range) and Chol (in the 0.2–0.3 nm^2 range) for the systems with 0, 2, and 4 inserted pyrene molecules (blue, red and green lines, respectively). From A to F, Chol mole fraction is 0, 0.05, 0.20, 0.40, 0.45 and 0.50. (For interpretation of the references to color in this figure legend, the reader is referred to the web version of this article.)

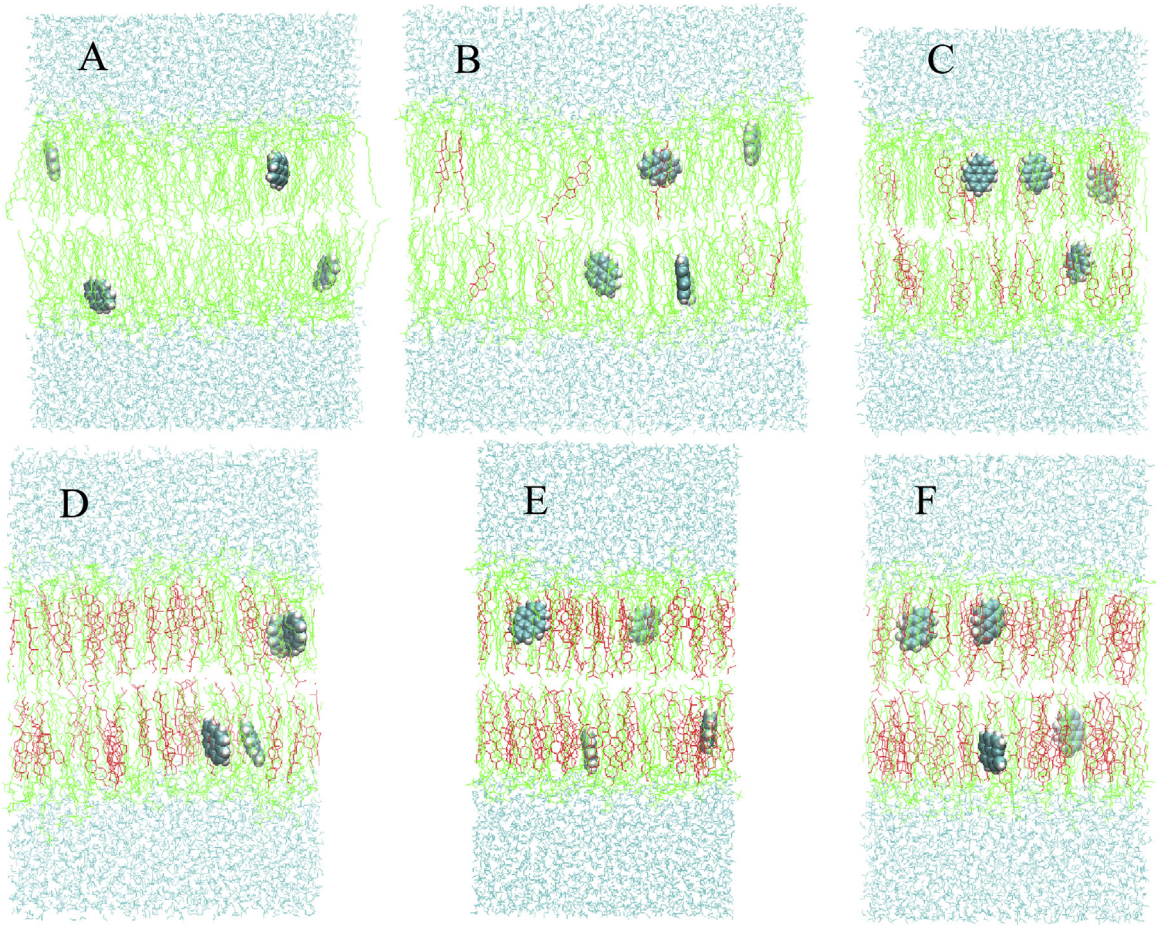

Fig. 3. Final 4-pyrene simulation structures. Water, PSM and Chol molecules are depicted as cyan, green and red lines, respectively. Pyrene molecules are shown as van der Waals representations. From A to F, Chol mole fraction is 0, 0.05, 0.20, 0.40, 0.45 and 0.50. (For interpretation of the references to color in this figure legend, the reader is referred to the web version of this article.)

case. A common feature to all simulations is that convergence of these parameters is achieved rapidly, indicating that equilibrium conditions are maintained throughout the runs.

Comparison with experimental values of area/lipid is very difficult, because of the extremely limited number of experimental studies. To our knowledge, no values at all have been reported for PSM/Chol bilayers, and a single value of 0.464 nm^2 has been reported for PSM from X-ray diffraction at 55 °C [36]. However, as noted by the authors of this work, this experimental area/lipid value was actually calculated from the measured bilayer periodicities, assuming a partial specific volume of 1.012 mL/g at 55 °C, corresponding to that of dipalmitoylphosphatidylcholine (DPPC). However, it is widely known that fluid DPPC and PSM bilayers have very different physical properties, and therefore, this "experimental" area/lipid value is probably incorrect. Indeed, experimental values for other saturated SM pure bilayers are considerably larger. For example, 0.55 nm^2 has been reported for *N*-stearoyl-SM [37]. These difficulties in comparison with experimental area/lipid values were also found and discussed in recent simulation studies [38,39]. For these reasons, we resort to comparing our molecular area values with results obtained from previous simulation studies.

The molecular area of pure PSM, averaged for $t > 50$ ns, is $(0.530 \pm 0.014)\,nm^2$, which agrees well with the values at $T = 323$ K of Niemelä et al. [23], who obtained $(0.52 \pm 0.01)\,nm^2$ (with the same force-field description), Metcalf and Pandit [38], who calculated $(0.533 \pm 0.004)\,nm^2$ (using slightly different united-atom parameters) and of Jämbeck and Lyubartsev [39], who reported $(0.541 \pm 0.004)\,nm^2$ (with an all-atom force field). Incorporation of either 2 or 4 pyrene molecules in pure PSM leads to no significant changes in PSM molecular area ($(0.530 \pm 0.013)\,nm^2$ and $(0.529 \pm 0.015)\,nm^2$ are obtained, respectively; see Fig. 2A).

Upon loading the PSM bilayer with increasing Chol content, two effects become apparent. First, the molecular area of PSM decreases slightly, reaching a minimum of $(0.493 \pm 0.012)\,nm^2$ for 20 mol% Chol, and increases slightly for higher Chol mole fractions, up to $(0.535 \pm 0.013)\,nm^2$ for 50 mol% Chol. One possible explanation to this non-monotonic variation is that, whereas relatively low amounts of Chol are capable of ordering to a small extent pure fluid PSM bilayers (similarly to the well-known effect on fluid PC bilayers), too much Chol would actually cause disruption the organization of PSM (possibly by reducing inter-PSM H bonding). However, this result is best interpreted cautiously at this stage, because artificial increases in molecular area of PC lipids have been observed at very high Chol fractions when using the area partitioning scheme employed here, due to its assumption that the area fractions of the two components are equal to their volume fractions [40]. In any case, it is clear from this analysis that the systems are conveniently equilibrated early on in the simulations and that the Chol condensing effect in PSM bilayers is much less pronounced than in their PC counterparts.

Second, while pyrene incorporation does not affect significantly lipid molecular areas for low Chol content, it is clear that, for higher Chol mole fractions (≥40 mol%), inclusion of pyrene induces an increase, which is most visible for the systems with four inserted probe molecules. For example, for 50 mol% Chol, $(0.535 \pm 0.013)\,nm^2$, $(0.539 \pm 0.013)\,nm^2$ and $(0.545 \pm 0.013)\,nm^2$

are obtained from the simulations with 0, 2 and 4 pyrene molecules, respectively. This is a first indication that pyrene may actually reduce the order of these systems, similarly to what we observed for POPC/Chol [16]. Although these variations are still within the statistical uncertainty associated with the calculations, it should be stressed that these values are averaged over all PSM molecules (not only those near the probe molecules), and local probe disordering effects are most probably more significant. This issue will be addressed in detail in connection to the lipid acyl chain order parameters (Section 3.2).

3.2. Mass density profiles

Fig. 4 shows mass density profiles along the bilayer normal of the different components of the 4-pyrene systems. The distance between density peaks increases from 4.0 nm for pure PSM to 4.4 nm for PSM/50 mol% Chol. This agrees well with the experimental peak separations in the electron density profiles, which vary between 4.2 nm for pure PSM and 4.5 nm for PSM/50 mol% Chol [36]. We believe that this comparison is more meaningful than that with the molecular areas reported in this experimental study, because, unlike the latter parameter, the experimental density peak separation does not depend on further assumptions.

Pure PSM bilayers are remarkably compact for fluid membranes, because of their characteristic strong intermolecular hydrogen bonding properties (e.g. [23] and references therein). Therefore, it is not surprising that, similarly to the modest variations in molecular area of the previous section, changes in the shape of the density profiles upon increasing Chol content are subtle. In particular, the distance between the center of the bilayer and the lipid/water interface (operationally defined as the plane for which lipid and water mass densities are equal) is remarkably invariant (mostly in the $z \sim 2.4$–2.5 nm range) for all systems shown in Fig. 4. This agrees with a recent synchrotron X-ray diffraction study, which reports that the thickness of liquid-ordered structures of sphingomyelin and cholesterol does not differ significantly from fluid phases of bilayers formed by the pure phospholipid [41]. Similarly, pyrene transverse distribution is virtually unaffected by the presence of Chol, and its maximum is in the range of $z \sim 1.2$–1.3 nm for all compositions. Small changes across the panels of Fig. 4 (e.g., deeper penetration into the bilayer center for some peaks) are probably not significant and reflect the behavior of individual pyrene molecules. The asymmetrical density profile of pyrene in the 20 mol% simulation is the result of a rare translocation event between monolayers during equilibration, which led to the final configuration of Fig. 3C with 3 (1) molecules in the upper (lower) leaflet, as well as 3:1 peak ratio in the pyrene distribution in Fig. 4C.

Paying close attention, one can observe that the water profile extends to slightly deeper locations in the membrane in the Chol-poor systems (0 and 5 mol% Chol), compared to those with 20 mol% or more of this component. This is most important regarding pyrene-reported polarity, and it is reflected in the degree of overlap of the pyrene and water distributions. A way to quantify this effect is to calculate an average water density sensed by pyrene, using the equation

$$\left\langle \rho(\text{water}) \right\rangle_{pyrene} = \frac{\int \rho_{pyrene}(z)\rho_{water}(z)dz}{\int \rho_{pyrene}(z)dz} \quad (1)$$

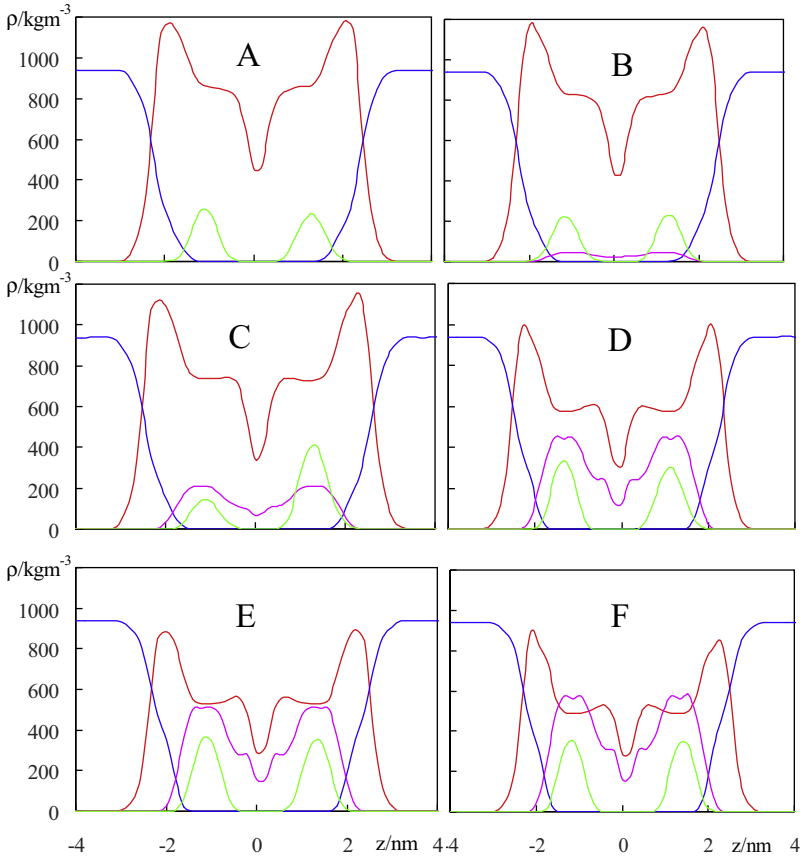

Fig. 4. Mass density profiles of PSM (red), Chol (magenta), pyrene (multiplied by 10 for better visualization; green), and water (blue) in the systems with 4 inserted pyrene molecules. From A to F, Chol mole fraction is 0, 0.05, 0.20, 0.40, 0.45 and 0.50. (For interpretation of the references to color in this figure legend, the reader is referred to the web version of this article.)

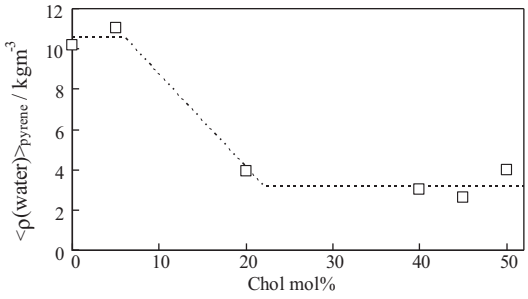

Fig. 5. Variation of the water density as sensed by pyrene (squares; calculated using Eq. (1)), for varying bilayer composition. The dotted line is just a guide to the eye.

This is illustrated in Fig. 5, which demonstrates that loading the bilayer with ≥20 mol% Chol reduces threefold the average density of water sensed by pyrene, compared to the Chol-free and 5 mol% Chol systems. The dotted line shown in the figure is reminiscent of the variation expected for liquid ordered/liquid disordered phase separation in the ~6–22 mol% composition range, as described from variations in lipid lateral diffusion coefficients measured by NMR [42]. No particular significance should be given to this fact, as two few compositions are addressed in this study, and especially because meso- or large-scale phase separation cannot be appreciated in atomistic simulations of bilayers made up of 100–200 lipid molecules.

3.3. PSM order parameters and Chol tilt in the bilayers

For our united atom forcefield, deuterium order parameters (S_{CD}) for saturated (S_{CD}^{sat}) and unsaturated (S_{CD}^{unsat}) carbons are determined from the order tensor elements S_{ab} using the following relations [43]:

$$-S_{CD}^{sat} = \frac{2}{3}S_{xx} + \frac{1}{3}S_{yy} \quad (2)$$

$$-S_{CD}^{unsat} = \frac{1}{4}S_{zz} + \frac{3}{4}S_{yy} + \frac{\sqrt{3}}{2}S_{xy} \quad (3)$$

where, in turn

$$S_{ab} = \frac{1}{2}\langle 3\cos\theta_a \cos\theta_b - \delta_{ab}\rangle \quad a, b = x, y, z \quad (4)$$

In the latter equation, θ_a (or θ_b) is the angle made by ath (or bth) molecular axis with the bilayer normal and δ_{ab} is the Kronecker delta (⟨ ⟩ denotes both ensemble and time averaging). The molecular axes for the nth CH_2 are [44]:

z: vector from C_{n-1} to C_{n+1};
y: vector perpendicular to z, lying in the plane defined by C_{n-1}, C_n, and C_{n+1}, pointing from C_n away from $1/2(C_{n+1}+C_{n-1})$;
x: vector perpendicular to both z and y.

Figs. 6 and 7 show the order parameters calculated for the sphingosine and palmitoyl chains (respectively) of PSM. The profiles

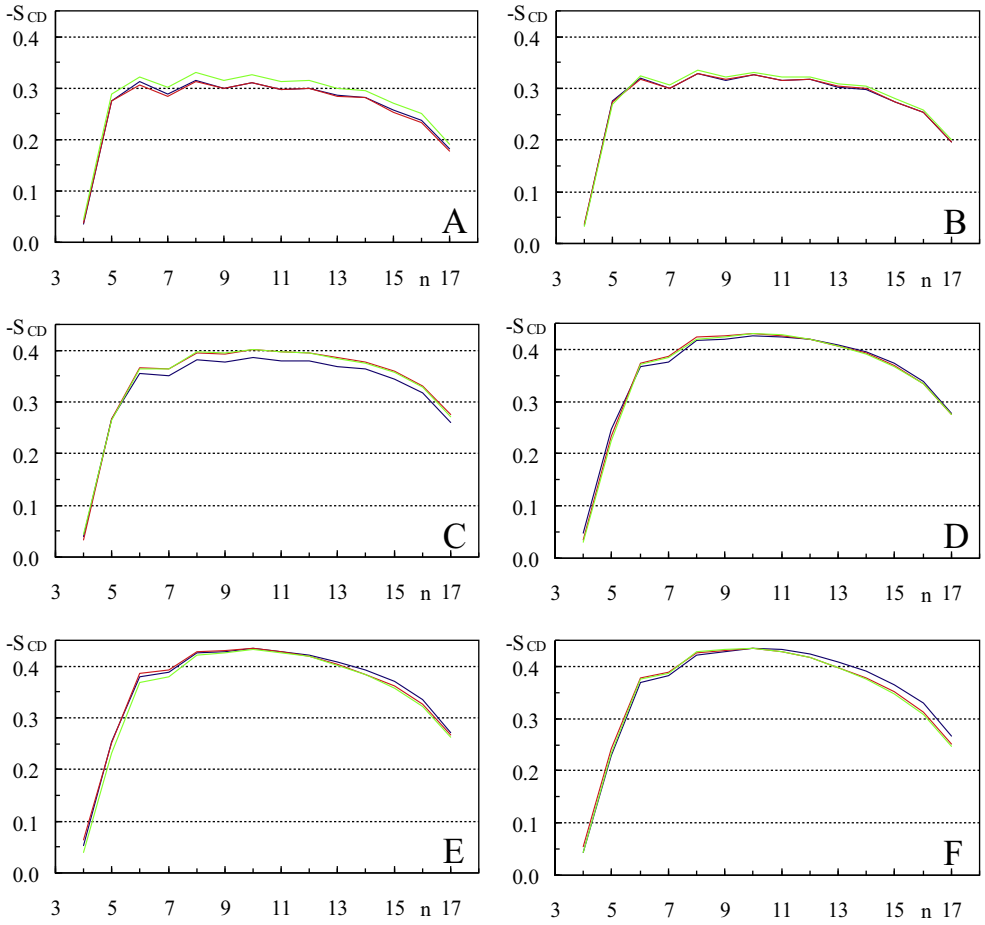

Fig. 6. Deuterium order parameter $-S_{CD}$ of the sphingosine chain of PSM, for the systems with 0, 2, and 4 inserted pyrene molecules (blue, red and green lines, respectively). From A to F, Chol mole fraction is 0, 0.05, 0.20, 0.40, 0.45 and 0.50. (For interpretation of the references to color in this figure legend, the reader is referred to the web version of this article.)

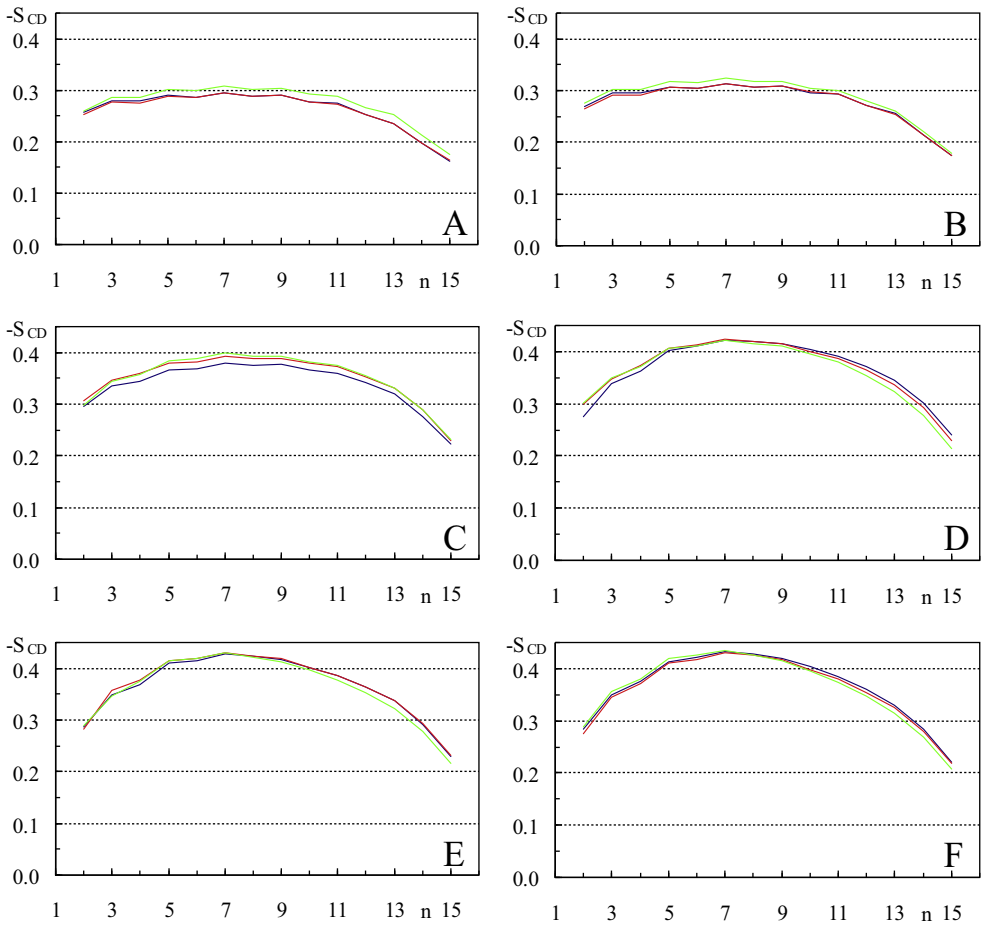

Fig. 7. Deuterium order parameter $-S_{CD}$ of the palmitoyl chain of PSM, for the systems with 0, 2, and 4 inserted pyrene molecules (blue, red and green lines, respectively). From A to F, Chol mole fraction is 0, 0.05, 0.20, 0.40, 0.45 and 0.50. (For interpretation of the references to color in this figure legend, the reader is referred to the web version of this article.)

obtained here for PSM and PSM/20 mol% Chol are somewhat higher than the experimental profiles obtained by ^{1}H NMR for PSM with perdeuterated palmitoyl chain [45], but agree very closely with those reported in other simulation works ([23] for PSM; [39] for both systems). Upon increasing the mole fraction of Chol in the system from 0 to 0.40, the order parameters for each segment increase steadily. Higher proportions of Chol lead to no discernible changes in the $-S_{CD}$ profiles. This confirms that the non-monotonic variation of the PSM molecular area was indeed artifactual, and that there is no evidence for a maximum in order for intermediate compositions.

Looking now at the effect of inserting pyrene molecules on the order parameter profiles, it appears that, for small to moderate Chol content (up to 20 mol%), pyrene may induce an increase in $-S_{CD}$, most visibly in the intermediate region of the chains (where pyrene predominantly resides) and in the 4-pyrene simulations. For 40 mol% Chol, no significant differences are observed, while for higher Chol concentration, loading the bilayer with pyrene molecule leads to a reduction in the order parameter, most notably in the lower end of the chains (where pyrene is rarely located, therefore leading to the appearance of voids underneath the probe molecules). Again, while this effect is modest overall, it could be significant in the vicinity of the probe molecules. To address this possibility, we calculated acyl chain order parameters for varying distance to the nearest pyrene probe. The results, illustrated in Fig. 8 for palmitoyl chains in the 2-pyrene simulations, show that whereas the effect of pyrene molecules on the order of nearby lipid molecules is small for pure PSM and 5 mol% Chol, a significant reduction is observed for the nearest lipid neighbors (located at <0.6 nm) at higher Chol concentrations. This is relevant for the interpretation of fluorescence measurements, because the probes only report on their local physical-chemical properties. Thus, it can be inferred that pyrene is an especially adequate probe of PSM/Chol membrane properties for low Chol fractions, but reports a lower local order for high Chol content, compared to the bulk bilayer.

We also examined the possibility of an effect of pyrene on the tilt of the long axis of Chol. We verified that very small changes in the angular distribution of this vector relative to the bilayer normal were produced upon loading each system with 2 or 4 pyrene molecules. While adding pyrene to a PSM/5 mol% Chol bilayer decreases the average tilt from 27.3° (no pyrene) to 26.0° (4 pyrene molecules), smaller variations (<0.5° in all cases) are obtained in the other systems, with visually indistinguishable distributions centered around ~24° for 20 mol% Chol and ~22° for ≥40 mol% Chol (data not shown).

3.4. Pyrene orientation and rotational dynamics

As illustrated in the snapshots of Fig. 3, pyrene tends to orient its long axis roughly along the bilayer normal. Fig. 9 shows the angular distributions of the long axis tilt. While a small fraction of conformations in the less ordered systems (0 and 5 mol% Chol) displays large tilt angles (visible in some of the probes' orientations in Fig. 3A and B), these are not very frequent molecular

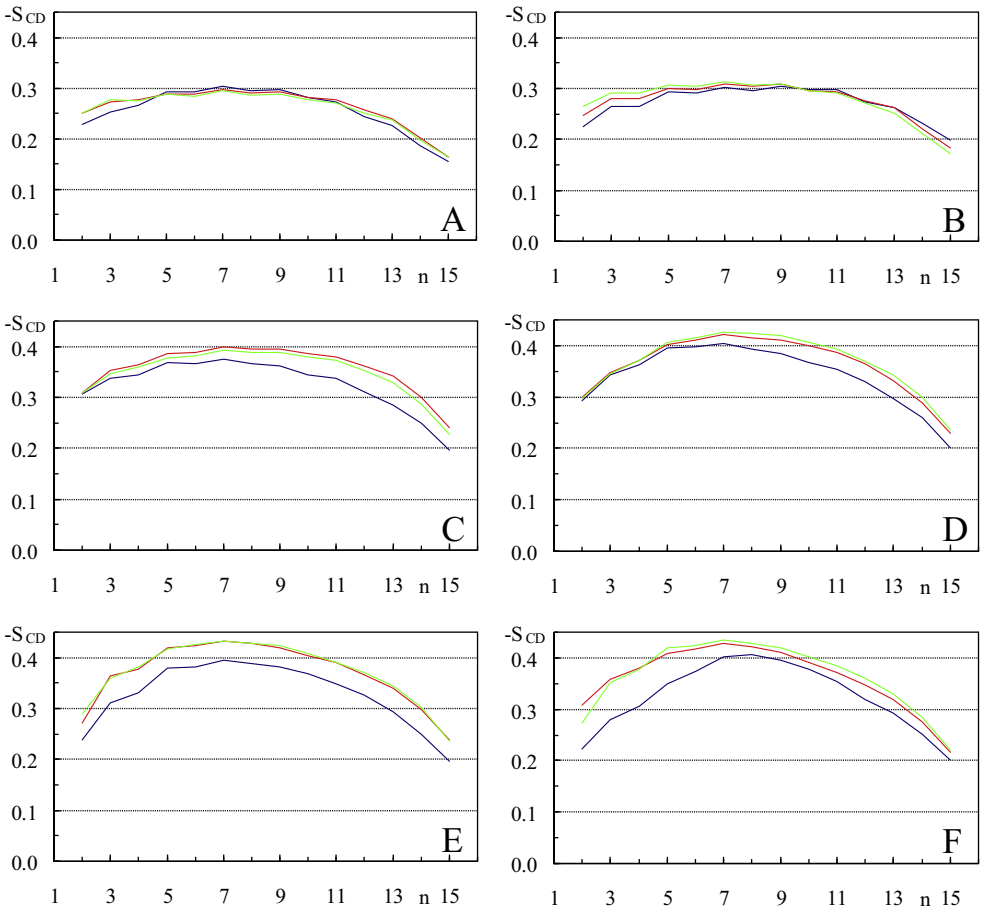

Fig. 8. Deuterium order parameter $-S_{CD}$ of the palmitoyl chain of PSM, for the systems with 2 inserted pyrene molecules. The blue, red and green lines are the order parameter profiles averaged for palmitoyl chains located at $R < 0.6$ nm, 0.6 nm $< R <$ 1.2 nm, and $R >$ 1.2 nm from the nearest pyrene molecule, respectively. From A to F, Chol mole fraction is 0, 0.05, 0.20, 0.40, 0.45 and 0.50. (For interpretation of the references to color in this figure legend, the reader is referred to the web version of this article.)

orientations. In accordance, the average tilt angles of the distributions shown in Fig. 9 (35–36° for 0–5 mol% Chol) are considerably smaller than those we obtained in POPC (48°) and even POPC/20 mol% Chol (41°), and almost comparable to that in POPC/40 mol% Chol (32°) [16]. For higher Chol content, the distributions shift progressively to lower tilt angles, albeit to a small extent (averages are 30°, 29°, 27° and 26° for 20, 40, 45 and 50 mol% Chol, respectively). In these latter compositions, the most significant feature is that highly tilted configurations (>60°) become highly improbable.

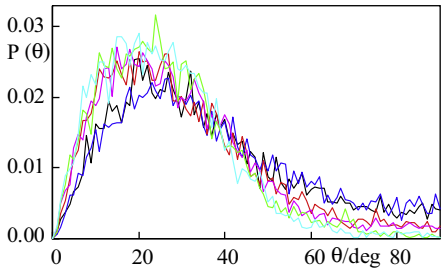

Fig. 9. Angular distributions of the pyrene long axis tilt, relative to the bilayer normal, for the 4 pyrene simulations with 0 (black), 5 (blue), 20 (red), 40 (magenta), 45 (green) and 50 (cyan) mol% Chol. (For interpretation of the references to color in this figure legend, the reader is referred to the web version of this article.)

Related to the question of the angular distributions is the amplitude and dynamics of pyrene rotation. Fig. 10 shows rotational autocorrelation functions (ACFs) of the long axis of pyrene for the different studied systems, defined as

$$C(t) = \langle P_2(\cos\theta(\xi))\rangle \quad (5)$$

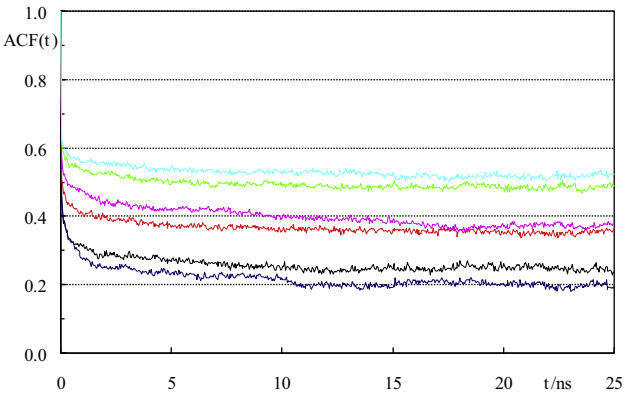

Fig. 10. Average rotational ACFs of the pyrene long axis in the simulations with 4 inserted pyrene molecules of the systems with 0 (black), 5 mol% (blue), 20 mol% (red), 40 mol% (magenta), 45 mol% (green) and 50 mol% (cyan) of Chol. (For interpretation of the references to color in this figure legend, the reader is referred to the web version of this article.)

where $\theta(\xi)$ is the angle between the probe long axis at times ξ and $t+\xi$, and $P_2(x)=(3x^2-1)/2$ is the second Legendre polynomial. Averaging is performed over ξ, which assuming a sufficiently ergodic trajectory, is an approximation of the ensemble average.

Fig. 10 shows only the rotational ACFs for the 4-pyrene systems, being the 2-pyrene curves similar (data not shown). Because averaging is carried out over a small number of probe molecules, they are most likely affected by limited sampling. Still, it is possible to observe that, in all cases, the ACFs drop almost instantly to ~0.4–0.6, probably because of very fast motions. Following this very steep decrease, further decay is slow and limited in extent, and a finite residual value of ACF is obtained in all cases. The rotational motion of pyrene can be described by a "wobbling-in-cone" model [46]. In this model, the probe has considerable orientational freedom for configurations where the long axis lies inside a cone of a given semi-angle θ_{max} (with cone axis normal to the bilayer plane), hence the very steep initial decrease. However, very tilted configurations ($\theta > \theta_{max}$) are forbidden (as the tilt angular distributions of Fig. 9 show, configurations with tilt angles $\theta > 60^\circ$ are indeed highly improbable), and hence the ACFs do not decay to zero even at long times. Higher ACF residual values correspond to narrower distributions, and are observed for the more ordered Chol-rich bilayers. From our simulations, there is little (probably non-significant) difference between the ACFs for 0 and 5 mol% Chol, as well as between those of the systems with 45 and 50 mol% Chol, with the other systems displaying an intermediate behavior. This steadily slower and more restricted rotational motion of the probe agrees with the increased order parameter profiles observed for the most Chol-enriched systems.

3.5. Pyrene lateral diffusion

Lateral diffusion coefficients D were calculated from the two-dimensional mean squared displacement (MSD), using the Einstein relation

$$D = \frac{1}{4}\lim_{t\to\infty}\frac{d\mathrm{MSD}(t)}{dt} \quad (6)$$

In turn, MSD is defined by

$$\mathrm{MSD}(t) = \langle||\vec{r}_i(t+t_0) - \vec{r}_i(t_0)||^2\rangle \quad (7)$$

where $\vec{r}_i$ is the (x, y) position of the center of mass of molecule i of a given species, the averaging is carried out over all molecules of this kind and time origins t_0. To eliminate noise due to fluctuations in the center of mass of each monolayer, all MSD analyses were carried out using trajectories with fixed center of mass of one of the monolayers, and the final result is averaged over the two leaflets. Fig. 11 shows MSD for pyrene and the host lipids for varying concentration of Chol, while the corresponding D values are given in Table 2.

The significance of MSD plots and accurate calculation of lateral diffusion in membranes remains, to a great extent, a controversial problem. It depends largely on the available time window [47,48]. Sampling problems are more important in lateral diffusion than in some other properties, because it involves large-scale motions of whole molecules rather than limited range/segmental motions (like those involved in lipid acyl chain or probe long axis orientation). For relatively short times, lipid diffusion (as perceived by MSD variation) is mainly due to conformational changes of the hydrocarbon chains rather than diffusion of the entire molecule [47], and therefore its meaning and its relationship to experimental observables are somewhat questionable. As the simulation time scale is extended, the possibility of observing true diffusional motion along the bilayer plane is increased. Our simulations span 300 ns, which is clearly enough for describing lateral diffusion in the more disordered systems, but possibly insufficient for Chol-rich bilayers,

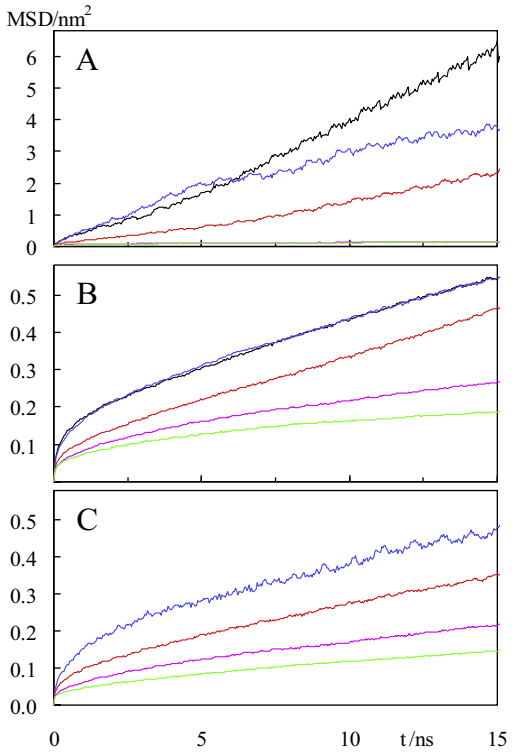

Fig. 11. Mean square displacements of pyrene (A; systems with 4 pyrene molecules), PSM (B; systems with no probe) and Chol (C; systems with no probe) for 0 (black), 5 mol% (blue), 20 mol% (red), 40 mol% (magenta), and 45 mol% (green) of Chol. (For interpretation of the references to color in this figure legend, the reader is referred to the web version of this article.)

where dynamics is considerably slowed down. Probably owing to this, MSDs of pyrene in the 50 mol% Chol system were unphysical, and the data shown exclude this composition.

As expected, the diffusion coefficients of the three species decrease with increasing Chol content and concomitant ordering of the bilayer. The values obtained for PSM are comparable (~2-fold lower) to the experimental data of Filippov et al. [42], obtained in egg yolk sphingomyelin/Chol. The reasons for the quantitative difference could be non-equivalence in bilayer properties arising from the difference in composition (according to the vendor [49], chicken egg yolk sphingomyelin has at least 3% of unsaturated fatty acids, which could account for increased fluidity), the above mentioned sampling difficulties, and/or small force field parameter issues. Accurate lateral diffusion coefficients are very difficult to obtain, because small changes in the bilayer order/fluidity lead to large variations in the D values. For example, the values measured by Filippov et al. [42] for $T = 323$ K are actually quantitatively very similar to ours calculated at 333 K. Most importantly, these authors report that loading with ~40 mol% Chol reduces D(SM) by a factor of 2–3, which is consistent with our observation that D(PSM) is reduced by less than an order of magnitude as Chol content is increased to 45 mol% (as expected for Chol-rich bilayers, which, although more ordered, retain their lateral diffusion-related fluidity [50]). According to our data, a similar variation occurs for Chol, whose D values in fact match closely those of PSM for a given bilayer composition.

This contrasts with the behavior of pyrene, for which increasing Chol mole fraction leads to a dramatic decrease of two full orders of magnitude in the lateral diffusion coefficient. Although precise estimation of D(pyrene) is difficult because of the small number of diffusing molecules used for averaging, even from visual inspection of Fig. 11 it is clear that Chol-induced ordering of the bilayer affects

Table 2
Lateral diffusion coefficients of pyrene (systems with 4 pyrene molecules), PSM, and Chol (systems with no probe).

Species	$D/(10^{-8}\ cm^2/s)$				
	0 mol% Chol	5 mol% Chol	20 mol% Chol	40 mol% Chol	45 mol% Chol
Pyrene	111 ± 11	54 ± 11	41 ± 9	1.2 ± 0.2	1.1 ± 0.2
PSM	5.4 ± 1.6	5.5 ± 1.5	6.3 ± 0.3	2.6 ± 1.0	1.4 ± 1.0
Chol	–	5.1 ± 0.5	4.2 ± 0.4	2.5 ± 0.4	1.6 ± 0.3

diffusion of pyrene to a much larger extent than those of PSM or Chol. The values of D of the three species are in fact similar for very high Chol concentration, and the "anomaly" is the fact that pyrene exhibits very fast diffusion in pure PSM (~20 times faster than PSM), which is readily reduced upon loading of the bilayer with Chol. Pyrene is a smaller apolar molecule (202.25 g/mol), which resides in the more disordered, hydrophobic region of the bilayer. Because it is unable to establish strong electrostatic/H bonding interactions with water/lipid components, unlike PSM and Chol, it possesses much more diffusional freedom than the latter for low-Chol systems. However, increasing the mole fraction of Chol leads to higher order parameter values, most notably in the middle region of the lipid chains, where pyrene is predominantly located. This is the probable reason why diffusion of pyrene is more severely reduced than that of the lipid species upon increasing Chol mole fraction.

4. Concluding remarks

4.1. Behavior of pyrene as a membrane probe

From the bilayer properties addressed in this study, pyrene exerts minor effects on PSM bilayer properties, and does not cause significant overall perturbation. It causes a slight, mainly local disordering of Chol-rich (≥20 mol%) bilayers, which does not preclude the use of pyrene in membrane studies. On the other hand, although the condensing effect of Chol is much less significant in PSM (very small area decrease/$-S_{CD}$ increase, as pure PSM already displays low molecular area/high $-S_{CD}$ profile) than in PC bilayers, pyrene dynamics is still greatly hindered upon adding Chol. This is probably because the ordering effect of Chol is most notably felt in the middle region of the lipid chains, where pyrene is predominantly located.

4.2. Polarity sensed by pyrene

Hydration sensed by pyrene in pure PSM bilayers is substantially low. For comparison, we calculated $\langle\rho(\text{pyrene})\rangle_{water}$, as defined in Eq. (1), for our data obtained in POPC and POPC/Chol [16]. The present values for PSM and PSM/5 mol% Chol (~10–11 kg m^{-3}) are well below those calculated in pure POPC (~45–50 kg m^{-3}) and even in POPC/20 mol% Chol (~25 kg m^{-3}). Remarkably, $\langle\rho(\text{pyrene})\rangle_{water}$ in PSM/Chol drops to even lower values (~3–4 kg m^{-3}) for high Chol mole fraction (≥20 mol%). This is an important contribution in the understanding of the physical properties of lipid rafts, which are mainly composed of SM and Chol. The apolar nature of these domains may be relevant, e.g. for their role in the sorting of membrane proteins.

This low hydration agrees with preliminary I_1/I_3 values obtained in POPC/Chol and egg SM/Chol multilamellar vesicles (0–45 mol% Chol) of varying lipidic composition [51]. The values obtained in POPC/Chol at 25 °C (which lie between 1.17 ± 0.01 for pure POPC, and 1.11 ± 0.01 for POPC/45 mol% Chol) are consistently higher than those measured for pure PSM in the fluid phase (which lie between 1.08 ± 0.01 at 45 °C and 1.06 ± 0.01 at 55 °C), in accordance with the simulation results. However, the experimental variation of I_1/I_3 with PSM/Chol composition at fixed temperature is not parallel to that of the simulated $\langle\rho(\text{pyrene})\rangle_{water}$. For the closest temperature addressed experimentally, 55 °C, I_1/I_3 shows little variation for ≤25 mol% Chol (while $\langle\rho(\text{pyrene})\rangle_{water}$ decreases markedly), and for higher Chol content it actually increases (while $\langle\rho(\text{pyrene})\rangle_{water}$ shows little change). While these variations are not divergent, they point to the possibility that alterations in I_1/I_3 may reflect other composition-influenced factors (that would, on their own, led to an increase in I_1/I_3 with Chol content) in addition to water penetration alone. Regarding this, it is noteworthy that, upon increasing Chol mole fraction, SM bilayers undergo a very significant increase in dipole potential [52]. It is tempting to hypothesize that membrane dipole potential could play an influence on I_1/I_3 similar to that of the solvent dipole moment in isotropic media, especially for such dehydrated environments as the interior of PSM/Chol bilayers. In this scenario, a continuous increase in dipole potential, combined with the variation in hydration felt by the probe as described here, could result in the experimentally determined dependence of I_1/I_3 on Chol-concentration.

Acknowledgements

L.M.S.L., A.M.T.M.C, and P.D.S. acknowledge funding by FEDER, through the COMPETE program, and by FCT (Fundação para a Ciência e a Tecnologia, Portugal), project reference FCOMP-01-0124-FEDER-010787 (FCT PTDC/QUI-QUI/098198/2008). P.D.S. acknowledges a grant under this same project. L.M.S.L. acknowledges additional funding by FCT, project reference PEst-OE/QUI/UI0313/2014. J.M. acknowledges the subsidy by national Portuguese funding through FCT – Fundação para a Ciência e a Tecnologia, projects ref. PEst-OE/EQB/LA0023/2013, and PTDC/QUI-BIQ/112943/2009.

References

[1] G. Cevc, D. Marsh, Phospholipid Bilayers: Physical Principles and Models, Wiley-Interscience, New York, 1987.
[2] D. Marsh, Handbook of Lipid Bilayers, second ed., CRC Press, Boca Raton, FL, 2013.
[3] O.H. Griffith, P.J. Dehlinger, S.P. Van, Shape of the hydrophobic barrier of phospholipid bilayers. Evidence for water penetration in biological membranes, J. Membr. Biol. 15 (1974) 159–192.
[4] D. Marsh, Membrane water-penetration profiles from spin labels, Eur. Biophys. J. 31 (2002) 559–562.
[5] C.D. Stubbs, C. Ho, S.J. Slater, Fluorescence techniques for probing water penetration into lipid bilayers, J. Fluoresc. 5 (1995) 19–28.
[6] T. Parasassi, E. Gratton, Membrane lipid domains and dynamics as detected by laurdan fluorescence, J. Fluoresc. 5 (1995) 59–69.
[7] A. Nakajima, Solvent effect on the vibrational structure of the fluorescence and absorption spectra of pyrene, Bull. Chem. Soc. Jpn. 44 (1971) 3272–3277.
[8] D.C. Dong, M.A. Winnik, The Py scale of solvent polarity. Solvent effects on the vibronic fine structure of pyrene fluorescence and empirical correlations with ET and Y values, Photochem. Photobiol. 35 (1982) 17–21.
[9] D.C. Dong, M.A. Winnik, The Py scale of solvent polarities, Can. J. Chem. 62 (1984) 2560–2665.
[10] E. Melo, J. Martins, Kinetics of bimolecular reactions in model bilayers and biological membranes. A critical review, Biophys. Chem. 123 (2006) 77–94.
[11] D. Arrais, J. Martins, Bilayer polarity and its thermal dependency in the ℓ_o and ℓ_d phases of binary phosphatidylcholine/cholesterol mixtures, Biochim. Biophys. Acta 1768 (2007) 2914–2922.
[12] L.M.S. Loura, J.P. Prates Ramalho, Fluorescent membrane probes' behavior in lipid bilayers: insights from molecular dynamics simulations, Biophys. Rev. 1 (2009) 141–148.
[13] L.M.S. Loura, J.P. Prates Ramalho, Recent developments in molecular dynamics simulations of fluorescent membrane probes, Molecules 16 (2011) 5437–5452.

[14] B. Hoff, E. Strandberg, A.S. Ulrich, D.P. Tieleman, C. Posten, ^{2}H-NMR study and molecular dynamics simulation of the location, alignment, and mobility of pyrene in POPC bilayers, Biophys. J. 88 (2005) 1818–1827.
[15] J. Čurdová, P. Čapková, J. Plášek, J. Repáková, I. Vattulainen, Free pyrene probes in gel and fluid membranes: perspective through atomistic simulations, J. Phys. Chem. B 111 (2007) 3640–3650.
[16] L.M.S. Loura, A.M.T. Martins do Canto, J. Martins, Sensing hydration and behavior of pyrene in POPC and POPC/cholesterol bilayers: a molecular dynamics study, Biochim. Biophys. Acta 1828 (2013) 1094–1101.
[17] K. Simons, E. Ikonen, Functional rafts in cell membranes, Nature 387 (1997) 569–572.
[18] K. Simons, D. Toomre, Lipid rafts and signal transduction, Nat. Rev. Mol. Cell Biol. 1 (2000) 31–39.
[19] D. Lingwood, K. Simons, Lipid rafts as a membrane-organizing principle, Science 327 (2010) 46–50.
[20] H.J.C. Berendsen, D. van der Spoel, R. van Drunen, GROMACS: a message-passing parallel molecular dynamics implementation, Comput. Phys. Commun. 91 (1995) 43–56.
[21] D. van der Spoel, E. Lindhal, B. Hess, G. Groenhof, A.E. Mark, H.J.C. Berendsen, GROMACS: fast, flexible and free, J. Comput. Chem. 26 (2005) 1701–1718.
[22] B. Hess, C. Kutzner, D. van der Spoel, E. Lindahl, GROMACS 4 algorithms for highly efficient, load-balanced, and scalable molecular simulation, J. Chem. Theory Comput. 4 (2008) 435–447.
[23] P. Niemelä, M.T. Hyvönen, I. Vattulainen, Structure and dynamics of sphingomyelin bilayer: insight gained through systematic comparison to phosphatidylcholine, Biophys. J. 87 (2004) 2976–2989.
[24] J. Domański, P. Stansfeld, M.S.P. Sansom, O. Beckstein, Lipidbook: a public repository for force field parameters used in membrane simulations, J. Membr. Biol. 236 (2010) 255–258.
[25] M. Holtje, T. Forster, B. Brandt, T. Engels, W. von Rybinski, H.D. Holtje, Molecular dynamics simulations of stratum corneum lipid models: fatty acids and cholesterol, Biochim. Biophys. Acta 1511 (2001) 156–167.
[26] http://www.gromacs.org/@api/deki/files/29/=cholesterol.tgz (accessed 21.06.14).
[27] J.R. Robalo, J.P. Prates Ramalho, L.M.S. Loura, NBD-labeled cholesterol analogues in phospholipid bilayers: insights from molecular dynamics, J. Phys. Chem. B 117 (2013) 13731–13742.
[28] B. Hoff, Aromaten in Phospholipid-Doppelschichten: Molekulardynamische Simulationen und Experimentelle Validierung (Ph.D. thesis), Universitätsverlag Karlsruhe, Karlsruhe, Germany, 2005.
[29] H.J.C. Berendsen, J.P.M. Postma, W.F. van Gunsteren, J. Hermans, Interaction models for water in relation to protein hydration, in: B. Pullman (Ed.), Intermolecular Forces, Reidel, Dordrecht, The Netherlands, 1981, pp. 331–342.
[30] H.J.C. Berendsen, J.P.M. Postma, A. DiNola, J.R. Haak, Molecular dynamics with coupling to an external bath, J. Chem. Phys. 81 (1984) 3684–3690.
[31] S. Miyamoto, P.A. Kollman, SETTLE: an analytical version of the SHAKE and RATTLE algorithms for rigid water models, J. Comput. Chem. 13 (1992) 952–962.
[32] B. Hess, H. Bekker, H.J.C. Berendsen, J.G.E.M. Fraaije, LINCS: a linear constraint solver for molecular simulations, J. Comput. Chem. 18 (1997) 1463–1472.
[33] U. Essman, L. Perela, M.L. Berkowitz, T. Darden, H. Lee, L.G. Pedersen, A smooth particle mesh Ewald method, J. Chem. Phys. 103 (1995) 8577–8593.
[34] W. Humphrey, A. Dalke, K. Schulten, VMD: visual molecular dynamics, J. Mol. Graph. 14 (1996) 33–38.
[35] C. Hofsäß, E. Lindahl, O. Edholm, Molecular dynamics simulations of phospholipid bilayers with cholesterol, Biophys. J. 84 (2003) 2192–2206.
[36] P.R. Maulik, G.G. Shipley, N-palmitoyl sphingomyelin bilayers: structure and interactions with cholesterol and dipalmitoylphosphatidylcholine, Biochemistry 35 (1996) 8025–8034.
[37] P.R. Maulik, P.K. Sripada, G.G. Shipley, Structure and thermotropic properties of hydrated *N*-stearoyl sphingomyelin bilayer membranes, Biochim. Biophys. Acta 1062 (1991) 211–219.
[38] R. Metcalf, S.A. Pandit, Mixing properties of sphingomyelin ceramide bilayers: a simulation study, J. Phys. Chem. B 116 (2012) 4500–4509.
[39] J.P.M. Jämbeck, A.P. Lyubartsev, Another piece of the membrane puzzle: extending slipids further, J. Chem. Theory Comput. 9 (2013) 774–784.
[40] M. Alwarawrah, J.A. Dai, J.Y. Huang, A molecular view of the cholesterol condensing effect in DOPC lipid bilayers, J. Phys. Chem. B 114 (2010) 7516–7523.
[41] P.J. Quinn, Structure of sphingomyelin bilayers and complexes with cholesterol forming membrane rafts, Langmuir 29 (2013) 9447–9456.
[42] A. Filippov, G. Orädd, G. Lindblom, The effect of cholesterol on the lateral diffusion of phospholipids in oriented bilayers, Biophys. J. 84 (2003) 3079–3086.
[43] J.P. Douliez, A. Leonard, E.J. Dufourc, Restatement of order parameters in biomembranes: calculation of CC bond order parameters from CD quadrupolar splittings, Biophys. J. 68 (1995) 1727–1739.
[44] D.P. Tieleman, D. van der Spoel, H.J.C. Berendsen, Molecular dynamics simulations of dodecylphosphocholine micelles at three different aggregate sizes: micellar structure and chain relaxation, J. Phys. Chem. B 104 (2000) 6380–6388.
[45] T. Bartels, R.S. Lankalapalli, R. Bittman, K. Beyer, M.F. Brown, Raftlike mixtures of sphingomyelin and cholesterol investigated by solid-state ^{2}H-NMR spectroscopy, J. Am. Chem. Soc. 130 (2008) 14521–14532.
[46] K. Kinosita Jr., S. Kawato, A. Ikegami, A theory of fluorescence polarization decay in membranes, Biophys. J. 20 (1977) 289–305.
[47] A.P. Lyubartsev, A.L. Rabinovich, Recent development in computer simulations of lipid bilayers, Soft Matter 7 (2011) 25–39.
[48] M. Javanainen, H. Hammaren, L. Monticelli, J.-H. Jeon, M.S. Miettinen, H. Martinez-Seara, R. Metzler, I. Vattulainen, Anomalous and normal diffusion of proteins and lipids in crowded lipid membranes, Faraday Discuss. 161 (2013) 397–417.
[49] http://www.avantilipids.com/index.php?option=com_content&view=article&id=437&Itemid=277&catnumber=860061 (accessed 21.06.14).
[50] O.G. Mouritsen, Life – As a Matter of Fat, Springer, New York, 2005.
[51] D. Arrais, J. Martins, Phospholipid/cholesterol binary mixtures: polarity variations with composition and temperature, Eur. Biophys. J. 40 (Suppl. 1) (2011) 195.
[52] T.J. McIntosh, S.A. Simon, D. Needham, C.H. Huang, Interbilayer interactions between sphingomyelin and sphingomyelin cholesterol bilayers, Biochemistry 31 (1992) 2020–2024.